Nanoscale Advances

ROYAL SOCIETY OF CHEMISTRY

PAPER

View Article Online
View Journal | View Issue

Check for updates

Cite this: *Nanoscale Adv.*, 2020, **2**, 2824

'Template-free' hierarchical MoS_2 foam as a sustainable 'green' scavenger of heavy metals and bacteria in point of use water purification†

Paresh Kumar Samantaray,[ab] Sushma Indrakumar,[b] Kaushik Chatterjee,[abc] Vipul Agarwal *[bd] and Suryasarathi Bose*[b]

Molybdenum disulfide (MoS_2), with its unique optical and electrical properties, has been explored for a variety of applications in the recent past. Still, its capabilities in point-of-use heavy metal ion removal remain to be explored. Herein, for the first time using a facile approach, we fabricated three-dimensional (3D) MoS_2 foam from exfoliated single to few-layered MoS_2 sheets for the selective exclusion of heavy metals and stringent bactericidal response. This foam was able to exclude 99.9% of Pb(II) and 98.7% of As(III) instantaneously and reduced more than 98% of bacteria *E. coli*. Moreover, the foam exhibits selective toxicity towards bacterial cells while showing no observable toxicity towards mammalian cells. The foam can be recycled and reused for at least five cycles under accelerated conditions and thus can be used for a promising non-cytotoxic, facile, and environmentally benign process for inline water remediation to remove heavy metal ions from the feed and as a potential antibacterial agent.

Received 28th November 2019
Accepted 5th May 2020

DOI: 10.1039/c9na00747d

rsc.li/nanoscale-advances

Open Access Article. Published on 06 May 2020. Downloaded on 2/23/2026 7:28:33 PM.
This article is licensed under a Creative Commons Attribution-NonCommercial 3.0 Unported Licence.

Introduction

Arsenic (As(III)) and lead (Pb(II)) remain in the top four toxic metal contaminants, the concentrations of which have seen a rapid increase in groundwater, posing a significant health risk in many countries like Argentina, Bangladesh, India, Mexico, Mongolia, Thailand, and Taiwan. The arsenic concentration in the groundwater of these countries ranges from 0.1 to over 2 ppm.[1] In the Indian subcontinent itself, the groundwater sources have an arsenic concentration of up to 0.3 ppm.[2,3] The main contributors of As(III) in the water system are industrial sources such as fertilizer and insecticide runoffs, by-products of oil extraction, and mining processes.[4] Above the permissible concentration As(III) is highly toxic which has been reported to cause skin damage, keratosis, heart disease, epigenetic modifications, diseases of the circulatory system and a wide variety of cancers.[5] Pb(II) is another highly toxic heavy metal, which gets rapidly absorbed in the bloodstream once ingested. In the north Indian region, the concentration of Pb(II) in water sources ranges from 0.008 to 0.11 ppm.[6] The induced toxicity of Pb(II) has been attributed to its enzyme chelation mechanism where Pb displaces the vital complexing elements such as iron, calcium, and zinc and thereby modifies the function of these enzymes.[7] Pb(II) induces severe damage to the kidneys and brain, by bypassing the blood–brain barrier, mimicking the calcium ion and causing wide-spread neuronal degeneration and eventuate into death.[8] Due to the low permissible limit, as recommended by the WHO, there have been considerable efforts towards the development of strategies for remediation of such toxic metals from groundwater and their detection using highly sensitive bio-sensing probes.[9] Thus, effective and efficient removal of these metals is a significant concern and a challenging task.

There are many approaches for faster reclamation of heavy metals like chemical precipitation, ion exchange, adsorption, membrane filtration, and electrochemical technologies.[10–15] Among these techniques, adsorption offers high-quality treatment of effluents and flexibility in design and operation. Engineered nanomaterials such as carbon-based materials (activated carbon, carbon nanotubes, and graphene/graphene oxide), magnetized materials (Fe_3O_4, and Ni) and polymeric materials (acrylamide-based hydrogels, polyethylene oxide, polyethylenimine, *etc.*) have shown potential as new adsorptive materials in removing organic as well as heavy metals from wastewater.[16–19] Among these materials, two-dimensional (2D) layered materials have been extensively researched in the field of water decontamination due to their excellent salt rejection and antibacterial properties.[20–30] In the recent past, most of the research has focused primarily on graphene oxide (GO) based

[a]*Centre for BioSystems Science and Engineering, Indian Institute of Science, Bangalore, India*

[b]*Department of Materials Engineering, Indian Institute of Science, Bangalore, India. E-mail: sbose@iisc.ac.in*

[c]*Manipal Institute of Regenerative Medicine, Manipal Academy of Higher Education, Bangalore, India*

[d]*Centre for Advanced Macromolecular Design (CAMD), School of Chemical Engineering, University of New South Wales, Sydney, NSW 2052, Australia. E-mail: agarwalvipul84@gmail.com*

† Electronic supplementary information (ESI) available. See DOI: 10.1039/c9na00747d

This journal is © The Royal Society of Chemistry 2020

Open Access Article. Published on 06 May 2020. Downloaded on 2/23/2026 7:28:33 PM.
This article is licensed under a Creative Commons Attribution-NonCommercial 3.0 Unported Licence.

membranes for water purification. These membranes have suffered from significant limitations such as: (i) introduction of friction against moving water compromising the structural integrity of the membrane over time; (ii) sensitivity towards changing pH; and (iii) probable hydration of the surface functional groups on GO leading to increases in the interlayer spacing and therefore, reduction in membrane selectivity to ions.[31,32]

MoS_2 has been envisioned to circumvent the limitations associated with GO-based membranes. Unlike GO, MoS_2 nanosheets lack surface functional groups making them inert to hydraulic resistance and swelling which could potentially lead to higher water flux.[29] Furthermore, the van der Waals' interaction between MoS_2 nanosheets provides greater structural integrity compared to hydrogen-bonded GO sheets, which in conjunction with high out-of-plane rigidity, could make them robust against the applied compression during the pressure-flow process. Further, research on the use of MoS_2 2D sheets in the form of stacked membranes for water filtration has just started emerging. It has been limited to desalination of particular species like sodium *etc.*[28,33] The scope of this material towards heavy metal studies is limited to highly sensitive biosensors for selective detection of As(III) in groundwater at a low limit of detection.[34] Conjugated MoS_2 composites have been employed to fabricate biosensors utilizing the specific properties of the different constituents of the composite for selective sensing of these toxic metal ions.[35,36] Recently, exfoliated MoS_2 nanosheets have been shown to rapidly interact with the Pb(II) and Pb(IV) species in water and yield a $PbMoO_{4-x}S_x$ product.[37] This work portrays the potential of using 2D MoS_2 nanosheets in water purification applications. However, in this study, the removal of Pb ions could only be achieved by surface adsorbing these 2D nanosheets on alumina or silica substrates. There has been no theoretical or experimental report demonstrating the applicability of 3D MoS_2 architectures in toxic heavy metal removal. Attempts towards the fabrication of 3D MoS_2 structures have been reported in some reports using metal or carbon-based materials for electro-catalytic or energy applications only.[38,39]

Herein, for the first time, we report a facile template-less approach for obtaining re-generative 3D MoS_2 foam from exfoliated MoS_2 nanosheets for rejection of toxic As(III) and Pb(II) species from water. This novel material can be deployed for reversible adsorption and desorption of toxic metal ions from water and to yield harsh bactericidal response to fecal coliforms. Our system, unlike other present adsorbents, can be reused with ease, and exhibits selective bacterial toxicity with no observable toxicity towards somatic cells. Taken together, this foam can be the next generation point of use system for quick water decontamination.

Results and discussion

MoS_2 was exfoliated with bovine serum albumin (BSA) as an exfoliating agent using ultra-sonication in a liquid exfoliation method.[40,41] The use of BSA has been reported to not only render the nanosheets biocompatible but also to act as a mild surfactant circumventing the inter-layer interactions and resulting in a stable colloidal dispersion of the nanosheets. The exfoliated MoS_2 nanosheets were observed to be single to few-layers as characterized by transmission electron microscopy (TEM) confirming the lateral dimension of ~50 nm (Fig. 1(a)). This was corroborated by atomic force microscopy (AFM) wherein the observed overall thickness was ~1.5 nm (Fig. 1(b)). It can be conclusively deduced from the height profile in Fig. 1(b) that exfoliation was successful, and there were 2–3 layers of MoS_2 sheets. (Thickness of MoS_2 monolayer is ~0.65 nm.[42]) UV/Vis spectrophotometric analysis exhibited characteristic peaks at 610 and 670 nm attributed to the B and A-exciton in the exfoliated MoS_2 nanosheets (Fig. 1(c)).[43] Another evidence of exfoliation can be obtained from the emergence of a characteristic photoluminescence (PL) bandgap (Fig. 1(d)).[44] PL analysis showcases the emergence of the bandgap exhibited by the prominent peak at around 1.91 eV (650 nm). The amount of BSA adsorption on the exfoliated sheets was quantified using BCA (bicinchoninic acid assay) analysis to be 296 ± 1.7 μg mL^{-1}. Taken together, the detailed characterization confirmed that the colloidal dispersion comprised predominantly single to few-layered MoS_2 nanosheets.

To exploit the versatility of the exfoliated sheets, hierarchical 3D MoS_2 foam was obtained by lyophilization of the colloidal dispersion of BSA exfoliated MoS_2 nanosheets (refer to Scheme 1). Fourier transform infrared spectroscopy (FTIR) was performed on the protein exfoliated foam and compared with that of the bulk MoS_2 to preliminarily characterize the presence of BSA (Fig. 2(a)). It was seen that the characteristic band of Mo–S at 469 cm^{-1} shifted to 475.6 cm^{-1} after protein-mediated exfoliation. Additionally, bands at 1524 cm^{-1} can be ascribed to the aromatic C=C stretching, 1720 cm^{-1} resulted from C=O stretching,[45,46] and 3281.5 cm^{-1} are due to NH stretching which confirmed the presence of BSA.[47] Furthermore, to visualize the surface morphology, scanning electron microscopy (SEM) was performed on the foam. The foam exhibited a 3D interconnected open network structure mediated by a low level of restacking of the nanosheets, which was expected from the lyophilization step (Fig. 2(b)). To ascertain the level of restacking, XRD was carried out on the fabricated foam. In Fig. 2(c), the following planes of MoS_2 (002), (100), (101), (102), (103), (006), (105), and (110) were observed corresponding to 2θ of 14.81°, 32.84°, 33.67°, 36.02°, 39.71°, 44.29°, 49.92°, and 58.64°, respectively. An additional broad peak at around 25° was also observed, which might be due to the presence of BSA.[48] The emergence and broadness of the peaks in the XRD confirmed the random restacking of the exfoliated nanosheets.[49] To study the impact of restacking on the intrinsic properties of the exfoliated MoS_2 nanosheets, PL was performed on the 3D foam. Notably, the foam retained the unique optical properties which are otherwise considered exclusive to the exfoliated single to few-layered MoS_2 nanosheets. The PL analysis exhibited two peaks at ~2.14 and 2.16 eV, which can be attributed to the trion and B-exciton peaks, respectively (Fig. 2(d)). The blue shift observed in the PL emission spectra can be attributed to the stress introduced in the system by the disordered stacking of the nanosheets upon lyophilization.[41,50]

Open Access Article. Published on 06 May 2020. Downloaded on 2/23/2026 7:28:33 PM.
This article is licensed under a Creative Commons Attribution-NonCommercial 3.0 Unported Licence.

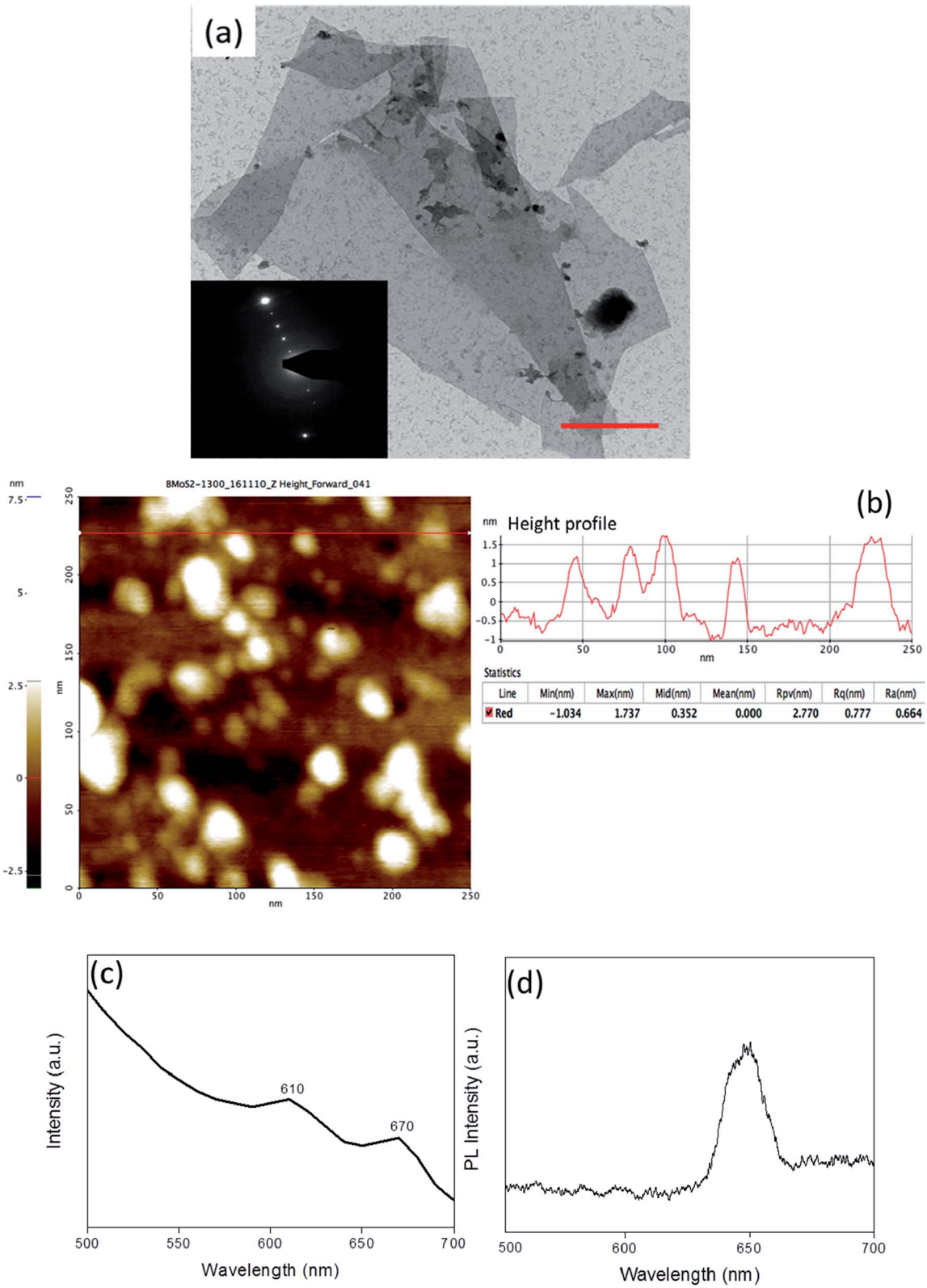

Fig. 1 Characterisation of the as-exfoliated MoS_2 sheets. (a) TEM image showing the exfoliated sheets (inset: selected area electron diffraction) (scale bar: 500 nm); (b) AFM image with the inset showing the height profile; (c) UV/Vis spectrum exhibiting the characteristic 610 and 670 nm peaks and (d) PL spectrum showing an energy bandgap of 1.9 eV (650 nm).

This journal is © The Royal Society of Chemistry 2020

Open Access Article. Published on 06 May 2020. Downloaded on 2/23/2026 7:28:33 PM.
This article is licensed under a Creative Commons Attribution-NonCommercial 3.0 Unported Licence.

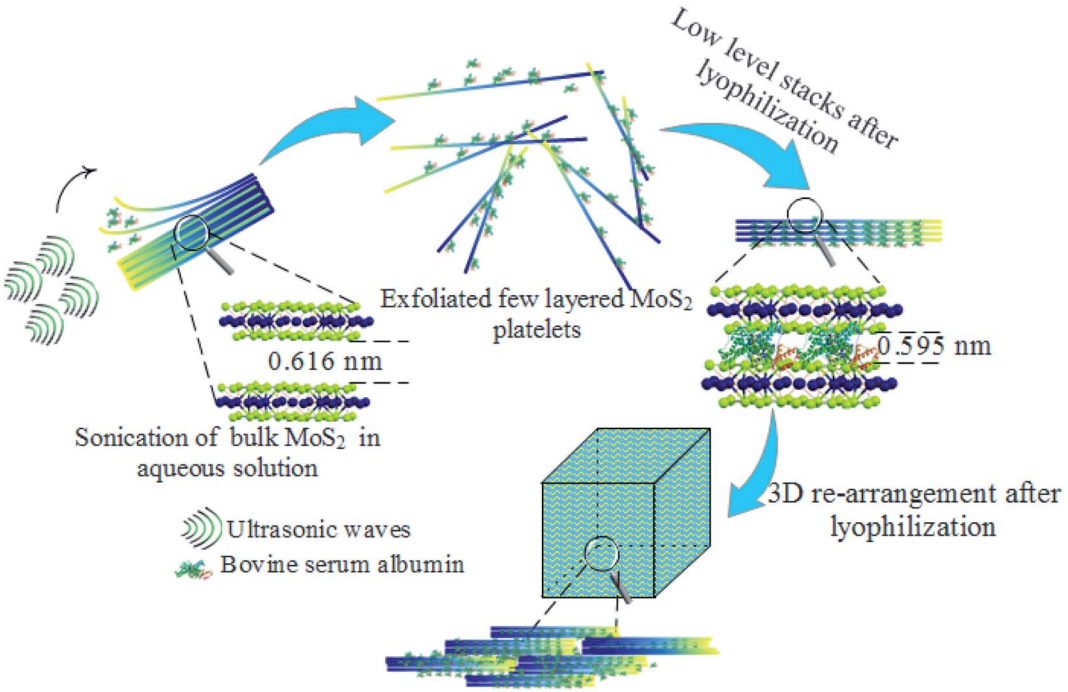

Scheme 1 Formation of 3D foam from few layers of MoS_2 nano-platelets using lyophilization.

3D foam as a point of use filter

The fabricated MoS_2 foam was assessed for point of use water remediation applications using As(III) and Pb(II) as model heavy metals by engineering an inline adsorption-based pre-filtration kit (refer to the ESI† for the method) with a continuous flow system. In this context, the exfoliated foam was exposed to accelerative studies with a dosage of 16.67–166.67 times the possible maximum concentration (0.3 ppm) of As(III) and 45.45–454.54 times the possible maximum concentration (0.11 ppm) of Pb(II). This was carried out to set a performance benchmark for this adsorbent and enable us to find the threshold cut off. Further, if the adsorbent can perform flawlessly under the accelerated condition, it is more likely that it would work under practical conditions (concentrations that are lower than that found in typical groundwater). Bulk MoS_2 was taken as a control for these experiments.

It was observed that the average rejection by exfoliated foam for all concentrations of Pb(II) was >98%. The average rejection by bulk MoS_2 for feed concentrations of 5 ppm, 10 ppm, 20 ppm, and 50 ppm were 86.3, 84.5, 82.7, and 82.4%, respectively ($n = 3$). In As(III), the average rejection for all concentrations of As(III) was >97%. The average rejection by the bulk MoS_2 control (refer to Fig. 3(a) and (b)) for 5 ppm, 10 ppm, 20 ppm and 50 ppm were 83.7, 82.9, 82.1 and 80.4% respectively ($n = 3$, and $p < 0.05$).

The permeation of water and other ionic molecules through nonporous materials like MoS_2 is generally facilitated *via* a interlayer *d*-spacing channels. It was inferred from the powder XRD data that the *d*-002 spacing of bulk MoS_2 was 0.616 nm, and with the exfoliated foam, it was slightly altered (*d*-002 spacing of exfoliated foam was 0.595 nm). The low level of re-stacking of the exfoliated nanosheets upon lyophilization with reduced *d*-spacing (protein stitched the adjacent MoS_2 sheets) generated interconnected pores, which provided the nano-channels for water permeation and trapped the metal ions (illustrated in Scheme 2). Herein, the critical factor that contributed towards quick removal of heavy metal impurities was size based sieving due to reduced *d*-spacing. The water, as well as heavy metal ions, was channelized through the slits as well as the interplanar spaces. Since the ions are more prominent in size, they are excluded at the interplanar space rather than ending up in the permeate resulting in enhanced removal of heavy metals. To corroborate this hypothesis, the foam after filtration was investigated using X-ray diffraction (XRD), and energy dispersive X-ray (EDX) mapping on SEM and XPS. Fig. 4(a) and (b) show the EDX mapping of the foam after Pb(II) and As(III) filtration, respectively. It can be seen that the ions are entrapped in the foam architecture. Furthermore, from the stacked XRD pattern of 3D foam and As(III) filtered foam (As(III)-foam) and Pb(II) filtered foam (Pb(II)-foam) it was observed that the (003) and (101) Bragg planes corresponding to 2θ values of 25.3° and 28.5° of arsenic metal in the As(III) state (ICDD ref. code: 96-900-9651) were obtained in the As(III)-foam. The (011) and (110) Bragg planes corresponding to 2θ values of 28.56° and 31.64° as observed in the case of Pb(II)-foam (Fig. 5(a)) are attributed to the +2 oxidation state of Pb (ICDD ref. code: 96-101-0978).

This was finally corroborated using XPS analysis wherein the binding energy of As $3d_{5/2}$ was obtained at 44.2 eV for As(III)-foam corresponding to the +3 oxidation state of arsenic.[51] Further, Pb $4f_{5/2}$ and Pb $4f_{7/2}$ peaks exhibited binding energies at 144.2 eV and 139.5 eV, respectively. This corresponds to the

Open Access Article. Published on 06 May 2020. Downloaded on 2/23/2026 7:28:33 PM.
This article is licensed under a Creative Commons Attribution-NonCommercial 3.0 Unported Licence.

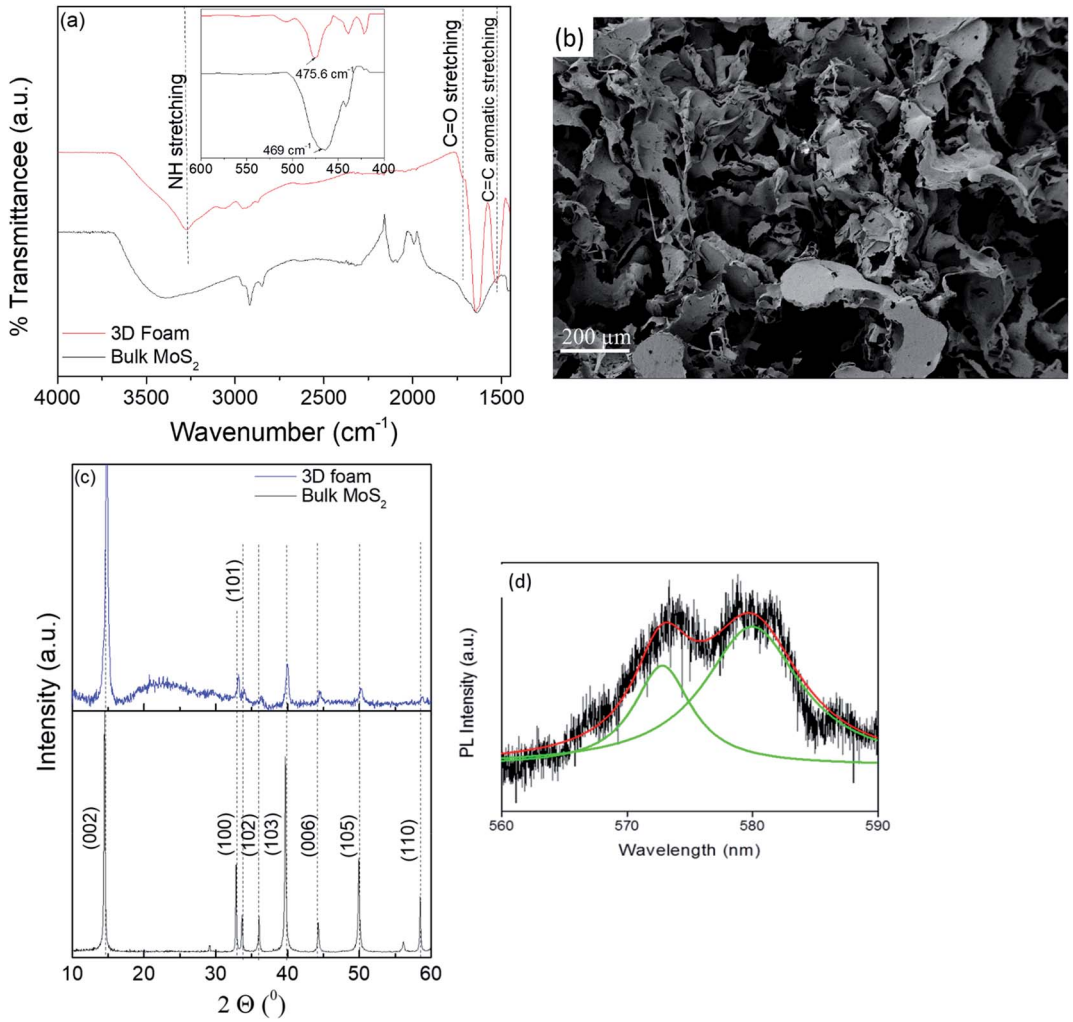

Fig. 2 Characterization of the fabricated 3D MoS_2 foam. (a) FTIR spectrum overlay of bulk MoS_2 and exfoliated foam; (b) SEM image showing the 3D connected network morphology (scale bar: 200 μm), (c) XRD spectrum of bulk MoS_2 and 3D foam; (d) photoluminescence (PL) spectrum showing convoluted (red) and de-convoluted (green) peaks at 579 nm and 574 nm corresponding to energy bandgaps of 2.14 and 2.16 eV, respectively.

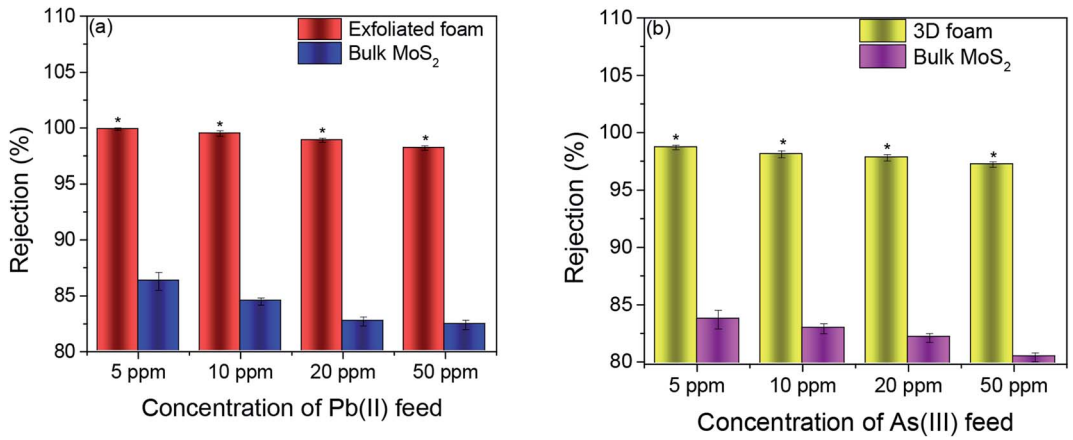

Fig. 3 (a) and (b) showing the water remediation response of the foam when exposed to the effluent containing increasing concentrations of the Pb(II) and As(III) contaminant, respectively. Data presented as average ± standard deviation with $n = 3$ and significance was set at $*p < 0.05$ using the Bonferroni *post hoc* test in one-way ANOVA analysis.

 This journal is © The Royal Society of Chemistry 2020

Open Access Article. Published on 06 May 2020. Downloaded on 2/23/2026 7:28:33 PM.
This article is licensed under a Creative Commons Attribution-NonCommercial 3.0 Unported Licence.

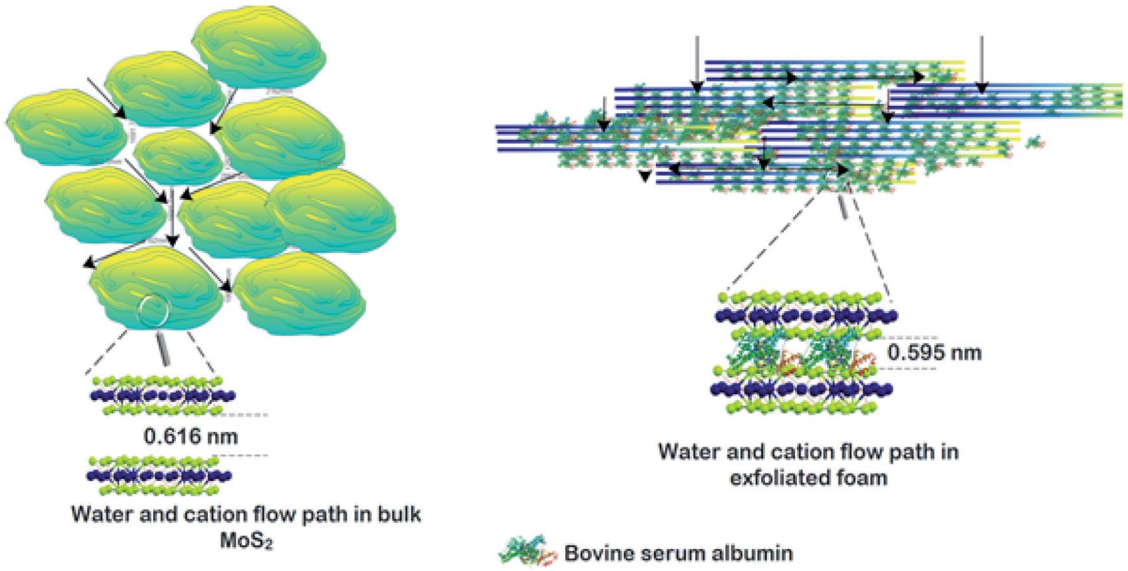

Scheme 2 Flow path for water and ions in bulk MoS_2 and exfoliated foam.

+2 oxidation state of lead (Fig. 5(b–d)).[52] Contrarily, bulk MoS_2 had bigger aggregates (primary and secondary agglomerates) bound together by van der Waals forces of interaction. These agglomerates were packed and rearranged randomly, and thus act as flow barriers to water molecules as well as metal ions. Although the water molecules as well as metal ions experience a resistive path while flowing through the material but, since the agglomerates are not broken, some ions elute through the least resistive path *i.e.* through the voids, and they channelize less through interlayer *d*-spacing channels which led to low rejection as compared to the 3D foam.

Recovery and re-use of 3D foam

To recover heavy metals like As(III) and Pb(II) after adsorption from water post-filtration, the foam was sonicated in double-distilled water for 30 minutes and centrifuged. The supernatant was isolated, and the concentration of heavy metal ions in the supernatant was determined using inductively coupled plasma optical emission spectroscopy (ICP-OES). The obtained centrifuged material was re-dispersed in 1 mg mL^{-1} BSA using sonication for 30 minutes and lyophilized to re-generate the foam. The regenerated foam was re-used for heavy metal removal

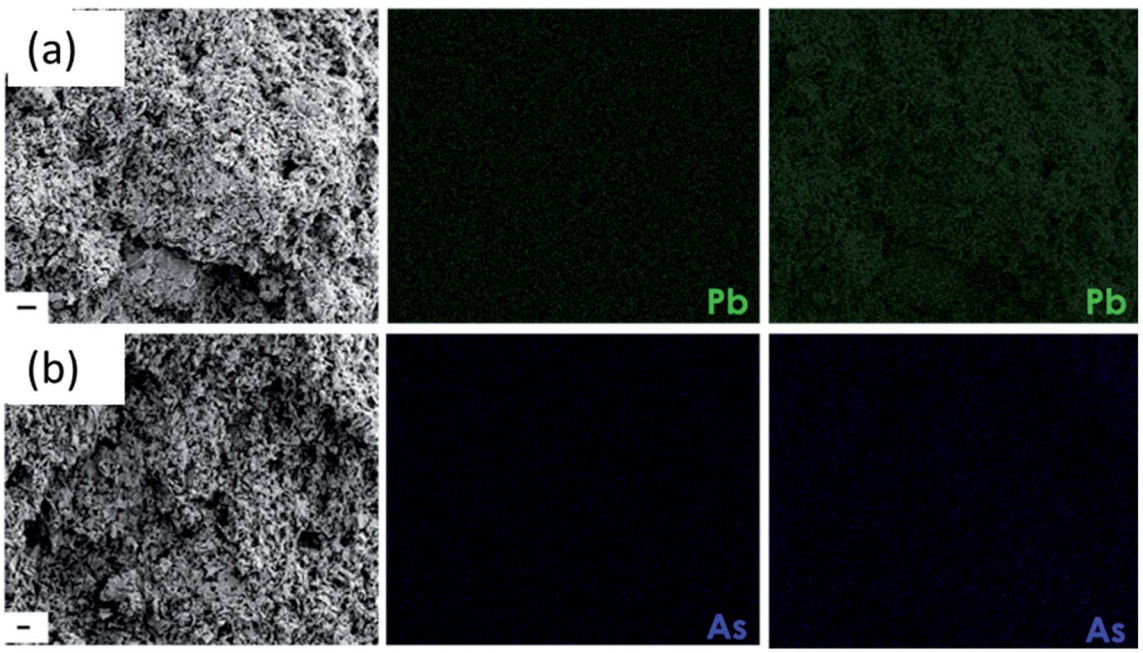

Fig. 4 (a) and (b) SEM image of the foam after filtration with the EDX mapping of the contaminant As and Pb ions (scale bar is 2 μm).

Open Access Article. Published on 06 May 2020. Downloaded on 2/23/2026 7:28:33 PM.
This article is licensed under a Creative Commons Attribution-NonCommercial 3.0 Unported Licence.

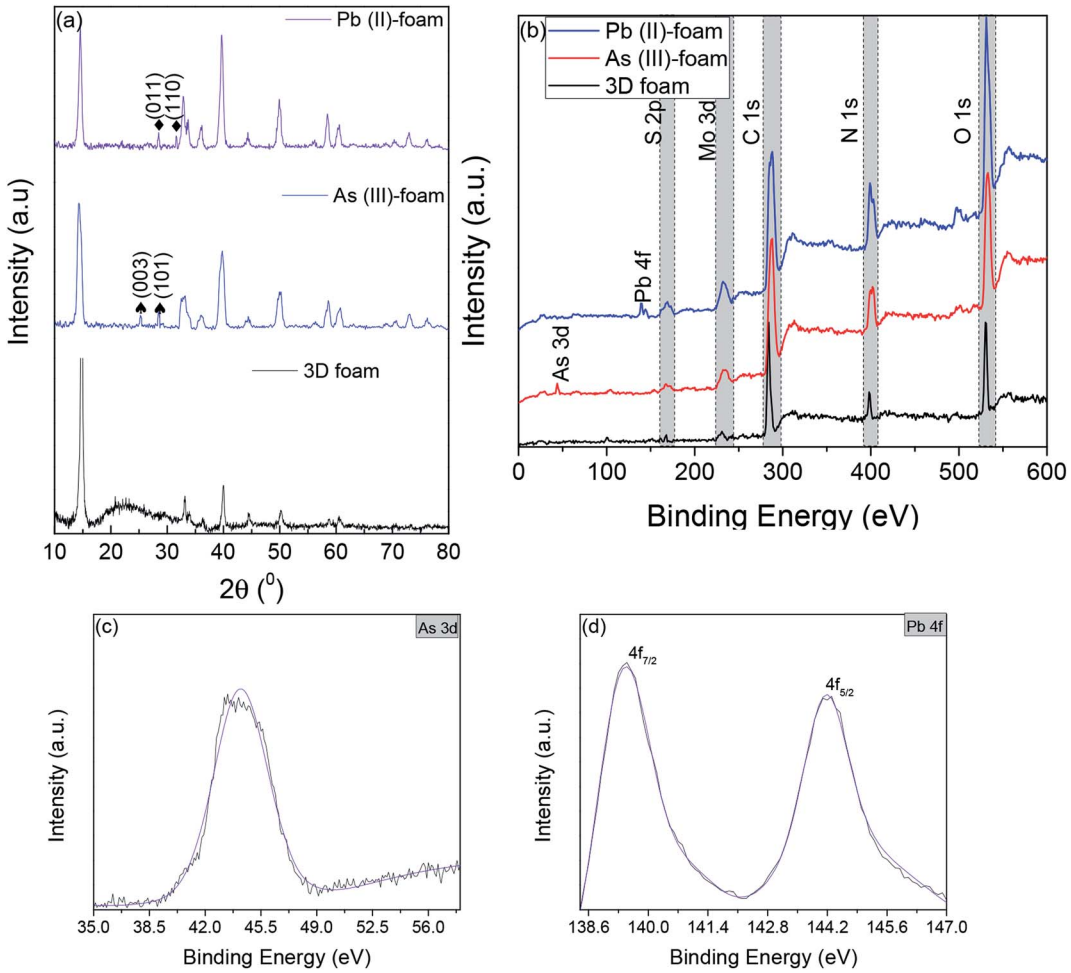

Fig. 5 (a) Stacked XRD spectra of the 3D foam after foam filtration experiments; (b) XPS wide spectra of the foam post filtration experiments showing the presence of Mo, S, As and Pb apart from C, N, and O which arises from BSA. (c) As 3d spectra for 3D foam post the As filtration experiment. (d) Pb 4f spectra for 3D foam post the Pb filtration experiment.

experiments. The concentration of heavy metal ions was fixed as 20 ppm (accelerated feed) for every experiment. Fig. 6(a) shows the recovery of heavy metals As(III) and Pb(II) for 5 cycles of re-use of the foam. Almost all the adsorbed heavy metal impurities were recovered entirely in all the 5 cycles of recovery experiments. Further, there was no statistical difference in the recovery of heavy metal ions in all the cycles. This efficient recovery of heavy metals makes the adsorbent surface available for the next cycle of re-use.

Fig. 6(b) shows the heavy metal removal efficiency of the 3D foam up to 5 cycles of re-use. It can be seen that even after passing the accelerated feed of 20 ppm through the system, the efficiency of heavy metal recovery was not compromised. Fig. 6(c) shows the digital micrograph of the "as obtained" foam after every cycle of re-use. It can be seen that the foam retained its properties even after cyclic re-dispersion and lyophilization.

The efficiency of the foam in the presence of interfering ions

In a practical situation, heavy metal ions are influenced by interfering ions. To evaluate the efficacy of our adsorbent to remediate these heavy metals in the presence of other interfering ions, we sampled tap water from our institute (Indian Institute of Science, Bangalore) with total dissolved solids (TDS) of 190 ± 28 ppm. Further, the sampled water majorly consisted of 36% Na^+ ions, 17% Mg^{2+} ions, 32% Ca^{2+} ions, and 8% of K^+ ions and the rest were trace elements like copper, iron, and zinc. This was then spiked with 0.3 ppm of As(III) and 0.1 ppm of Pb(II), respectively.

Fig. 7 shows the heavy metal removal efficiency for tap water spiked with As(III) and Pb(II), respectively. The control for these tests was bulk MoS_2. In the presence of interfering ions, there was a marginal reduction in efficiency in arsenic and lead removal. However, the As(III) removal was recorded to be 98.76% while Pb(II) removal was recorded to be 98.97% which strictly meets the current standards set by the WHO for arsenic and lead, respectively.[53]

Table S1 (refer to the ESI)† exhibits the comparison of our reported MoS_2 foam with similar systems reported in the literature depicting adsorption efficiency of 2D material foam-based adsorbents for remediating lead and arsenic-based contaminants. It is important to note that all the studies are based on

 This journal is © The Royal Society of Chemistry 2020

Open Access Article. Published on 06 May 2020. Downloaded on 2/23/2026 7:28:33 PM.
This article is licensed under a Creative Commons Attribution-NonCommercial 3.0 Unported Licence.

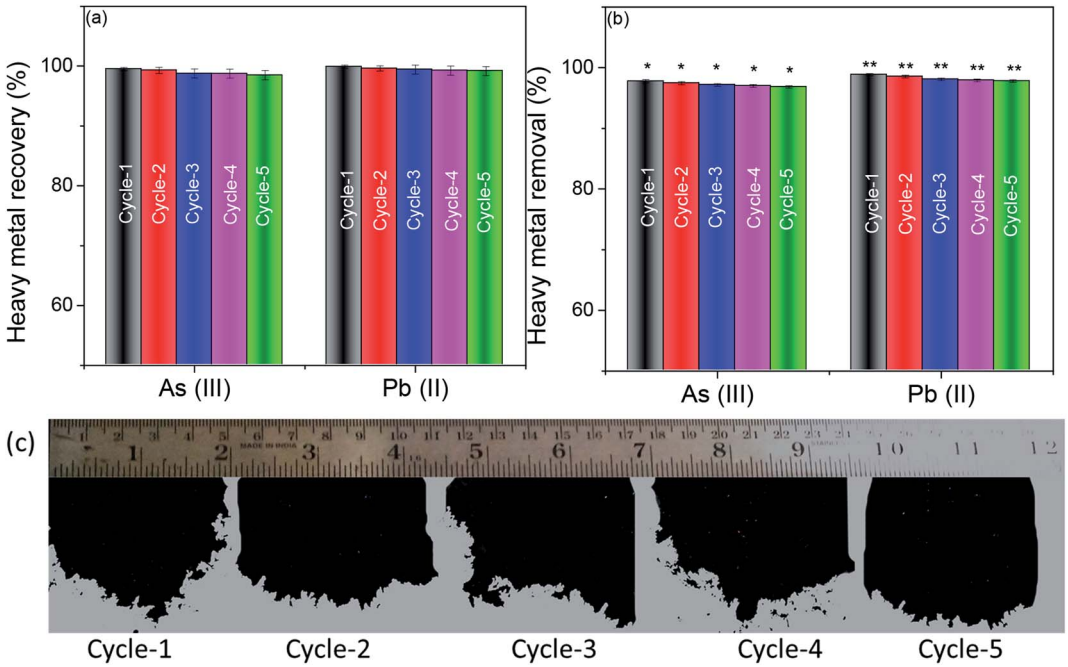

Fig. 6 (a) Heavy metal recovery from the adsorbent after 5 cycles of usage. (b) Heavy metal removal capabilities of the 3D foam for 5 cyclic usages. * and ** indicate statistical significance across arsenic rejection and lead rejection respectively with $n = 3$, and $p < 0.05$ using one-way ANOVA and Bonferroni *post hoc* analysis. (c) Digital micrograph of foams obtained after re-dispersion and lyophilization cycle of re-use.

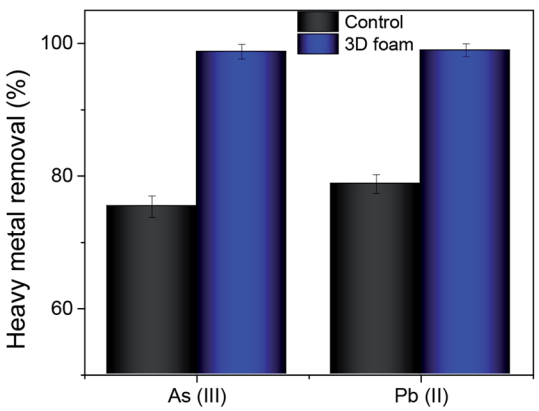

Fig. 7 Heavy metal removal efficiency of 3D foam with tap water spiked with As(III) and Pb(II) contaminants. Data presented as average ± standard deviation with $n = 3$.

graphene as the base 2D material, and there is no reported work on either MoS_2 or MoS_2 based foams for remediating toxic lead and arsenic-based contaminants. Further, the reported efficiencies of lead and arsenic in this work are considerably superior to the existing literature reports.

The efficacy of the 3D foam to remediate bacterial contamination was demonstrated herein using *E. coli* ATCC 25922 as a model strain. Fig. 8(a) and (b) show the effects of concentration and incubation time on the bacterial cell viability for 3D foam and bulk MoS_2, respectively. It can be seen from Fig. 8(a) and (b) that the reduction in bacterial cell viability was significantly more for 3D foam as compared to bulk MoS_2 as a function of concentration as well as incubation time. The mechanism of bacterial reduction by the exfoliated MoS_2 sheets is mediated through the generation of reactive oxygen species,[22,54,55] and by scissoring effects.[56,57] For this reason, a maximum average bacterial reduction of 98.8 ± 1.5% was seen for 200 μg mL^{-1} concentration of dispersed 3D foam for a 4 h incubation time. In contrast, for the bulk MoS_2, only 42.2 ± 1.8% average reduction was seen for the same concentration and incubation time. To decipher the mechanism behind the antibacterial activity, we explored reactive oxygen species (ROS) using the dichlorodihydrofluorescein diacetate (DCFH-DA) assay[58–60] (see the ESI† for mode of action) at 200 μg mL^{-1} concentration of the material. Fig. 8(c) exhibits time dependent increase in the amount of ROS for both foam and the control MoS_2 bulk material. The rate of increase in the ROS level obtained correlated well with the time dependent reduction in bacterial cell viability, which indicates that the sharp edges of the nanosheets in the foam would have potentially induced intracellular membrane stress before scissoring the bacterial cells thereby causing cell death.

One of the key challenges in the fabrication of membrane filters or any other filtration material is their impact on the biological and ecological environments. Such exposure was predominantly mediated by leaching of the material either through the compromised structural integrity with time or hydraulic rupture. Furthermore, it is important to elucidate whether the toxicity of the fabricated foam is selective and limited only to microbial cells. To this end, we evaluated the *in vitro* cytotoxicity of the re-dispersed foam in immortalized

Open Access Article. Published on 06 May 2020. Downloaded on 2/23/2026 7:28:33 PM.
This article is licensed under a Creative Commons Attribution-NonCommercial 3.0 Unported Licence.

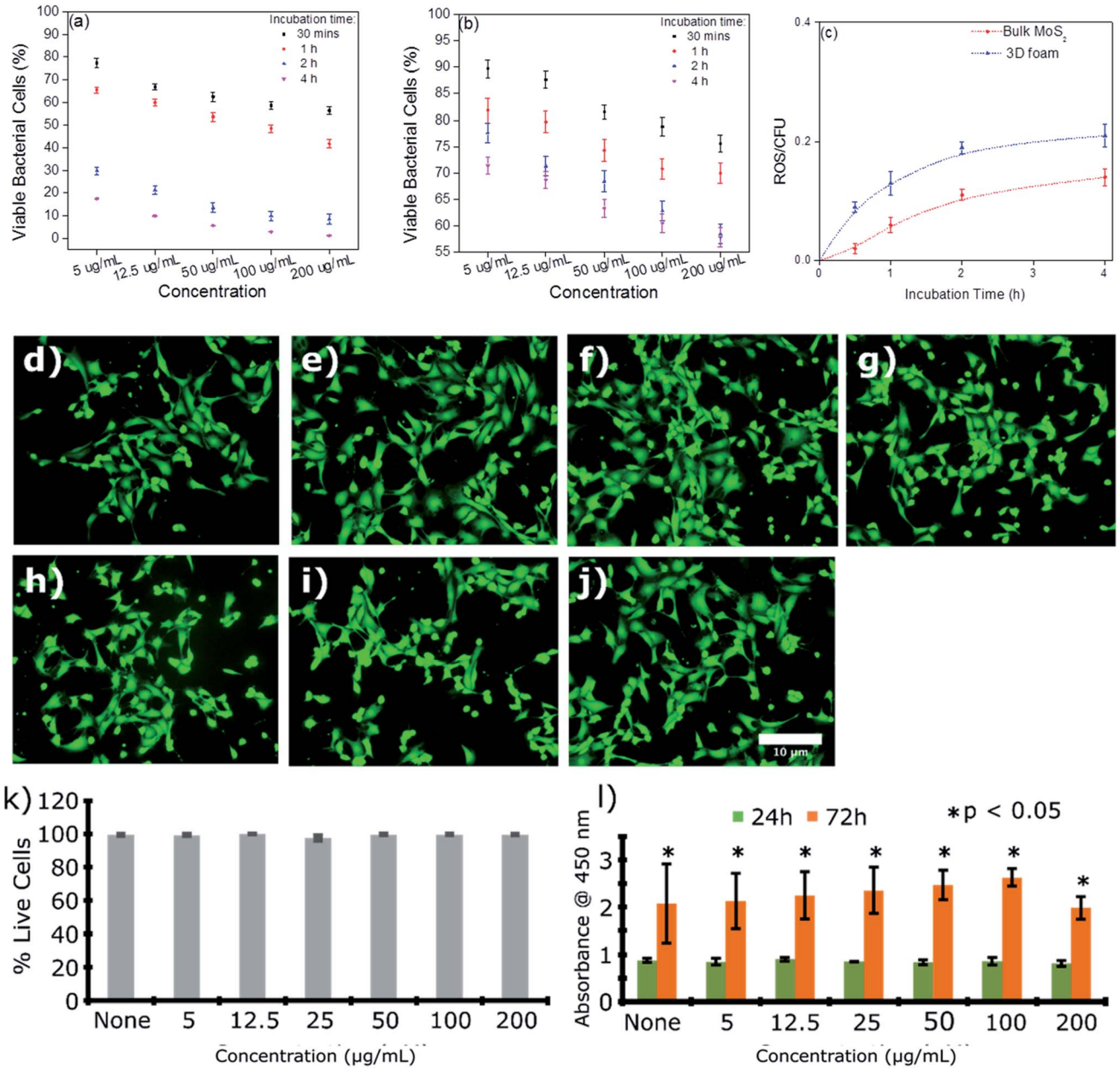

Fig. 8 Bacterial cell (*E. coli*) toxicity of the re-dispersed foam. (a) and (b) Percentage cell viability showing the response to the increasing concentrations of the foam and bulk MoS_2 material, respectively($n \geq 3$); (c) quantification of the reactive oxygen species (ROS) experienced by bacterial cells when exposed to the bulk material and re-dispersed foam with time ($n \geq 3$) biocompatibility of the foam towards the mouse lymphoid endothelial cell line (SVEC) cells. (d–j) Representative fluorescence images showing some live and dead cells in the culture. SVEC cells were incubated on (d) none (untreated control), (e) 5 μg mL^{-1}, (f) 12.5 μg mL^{-1}, (g) 25 μg mL^{-1}, (h) 50 μg mL^{-1}, (i) 100 μg mL^{-1}, and (j) 200 μg mL^{-1}. Scale bar: 10 μm. Cells were stained using Calcein AM/ethidium bromide I staining where live cells were stained fluorescent green while dead cells fluorescent red;[61,62] (k) quantification of the live/dead cell viability assay showing the percentage of live cells in the culture treated with increasing concentrations of the re-dispersed foam ($n = 4$); (l) WST-1 cell proliferation assay showing significant proliferation throughout 72 h. Data presented as mean ± SEM ($n = 5$). Significance was set at $*p < 0.05$ using one-way ANOVA and Bonferroni *post hoc* analysis.

mouse lymphoid endothelial (SVEC) cells. Cytotoxicity and cell viability were assessed using WST-1 and live/dead assays (Fig. 8(d–j)). No change was observed in the growth and viability of the SVEC cells at any of the concentrations studied. Moreover, fluorescence imaging of the cells revealed no change in the cell morphology, highlighting the biocompatibility of the nanosheets (Fig. 8(d–j)).

Discussion

3D foams are indeed versatile adsorbents in water remediation strategies. Owing to their superior performance and ease of deployment, 3D foams offer 'point of use' support for remediation applications. In the current literature, 2D material-based foams are generally obtained using a support template, and the

 This journal is © The Royal Society of Chemistry 2020

Open Access Article. Published on 06 May 2020. Downloaded on 2/23/2026 7:28:33 PM.
This article is licensed under a Creative Commons Attribution-NonCommercial 3.0 Unported Licence.

current literature majorly explores graphene oxide (GO) based adsorbents (refer to the ESI, Table S1†). However, since the application is water remediation and the 2D material should not be affected by undue swelling, which leads to an increase in interlayer *d*-spacing, GO-based foams can have drawbacks. GO sheets swell in the presence of water molecules leading to an increase in the interlayer *d*-spacing which has been reported to compromise the performance of GO-based foams.[57] Interlayer *d*-spacing plays a critical role in rejecting and blocking metal ions and other contaminants *via* a sieving mechanism.

Herein, we addressed this issue by using MoS_2 which is resistant to swelling due to lack of any surface functional groups. Using BSA as an exfoliating agent, an effective exfoliation of MoS_2 nanosheets was achieved. The exfoliated sheets were lyophilized to obtain a 3D MoS_2 foam. These foams were then used as a point of use adsorbent to remediate arsenic and lead-based heavy metal contaminants. Not only were the foams effective at an accelerated concentration up to 50 ppm, but the foams were also easily re-useable and were effective in the presence of interfering ions as well. Further, these foams were effective in remediating pathogenic bacteria *E. coli* and exhibited no observable cytotoxicity towards SVEC mammalian endothelial cells.

Conclusions

To summarize, herein, we fabricated 3D MoS_2 foam by lyophilization from the protein-mediated exfoliated nanosheets of MoS_2. The technique was robust and environmentally benign and retained the chemical properties of the exfoliated nanosheets. The 3D foam exhibited excellent removal efficiency for As(III) and Pb(II) with an average rejection of 98.7 and 99.9%, respectively. Furthermore, the foam demonstrated significant dose and exposure time-dependent antibacterial efficacy against *E. coli* mediated through the ROS-dependent pathway. The maximum reduction of *ca.* 98% in bacterial cell viability was observed at 200 μg mL^{-1} concentration of the re-dispersed foam during a 4 h exposure time. The foam was observed to induce selective toxicity towards the bacterial cells while being non-toxic towards mammalian cells. Taken together, the rejection of heavy metal ions, as well as the bactericidal response with no visible cytotoxicity, makes this foam an excellent material for point of use water remediation.

Conflicts of interest

There are no conflicts of interest to declare.

Acknowledgements

The authors would like to acknowledge the Department of Science and Technology, India for the financial support and The Centre for Nano Science and Engineering (CeNSE) at IISc for instrumental support. V. A. would like to acknowledge the National Health and Medical Research Council (NHMRC) (GNT1139060), Australia, for an Early Career Fellowship and UNSW-MAHE research collaboration seed grant.

References

1 R. Harisha, K. Hosamani, R. Keri, S. Nataraj and T. Aminabhavi, *Desalination*, 2010, **252**, 75–80.
2 D. Chakraborti, B. Das, M. M. Rahman, U. K. Chowdhury, B. Biswas, A. Goswami, B. Nayak, A. Pal, M. K. Sengupta and S. Ahamed, *Mol. Nutr. Food Res.*, 2009, **53**, 542–551.
3 P. K. Samantaray, S. Baloda, G. Madras and S. Bose, *ACS Sustainable Chem. Eng.*, 2019, **7**, 18775–18784.
4 M. Hua, S. Zhang, B. Pan, W. Zhang, L. Lv and Q. Zhang, *J. Hazard. Mater.*, 2012, **211**, 317–331.
5 K. Jomova, Z. Jenisova, M. Feszterova, S. Baros, J. Liska, D. Hudecova, C. Rhodes and M. Valko, *J. Appl. Toxicol.*, 2011, **31**, 95–107.
6 K. P. Singh, A. Malik, V. K. Singh, D. Mohan and S. Sinha, *Anal. Chim. Acta*, 2005, **550**, 82–91.
7 P. B. Tchounwou, C. G. Yedjou, A. K. Patlolla and D. J. Sutton, in *Molecular, clinical and environmental toxicology*, Springer, 2012, pp. 133–164.
8 P. K. Samantaray, S. Baloda, G. Madras and S. Bose, *J. Mater. Chem. A*, 2018, **6**, 16664–16679.
9 H. N. Kim, W. X. Ren, J. S. Kim and J. Yoon, *Chem. Soc. Rev.*, 2012, **41**, 3210–3244.
10 Y.-H. Wang, S.-H. Lin and R.-S. Juang, *J. Hazard. Mater.*, 2003, **102**, 291–302.
11 T. A. Kurniawan, G. Y. Chan, W.-H. Lo and S. Babel, *Chem. Eng. J.*, 2006, **118**, 83–98.
12 B. Pan, B. Pan, W. Zhang, L. Lv, Q. Zhang and S. Zheng, *Chem. Eng. J.*, 2009, **151**, 19–29.
13 B. Boruah, R. Gupta, J. M. Modak and G. Madras, *J. Photochem. Photobiol., A*, 2019, **373**, 105–115.
14 B. Boruah, R. Gupta, J. M. Modak and G. Madras, *Nanoscale Adv.*, 2019, **1**(7), 2748–2760.
15 P. K. Samantaray, G. Madras and S. Bose, in *Next Generation Biomanufacturing Technologies*, ACS Publications, 2019, pp. 321–351, DOI: 10.1021/bk-2019-1329.ch014.
16 M. J. Sweetman, S. May, N. Mebberson, P. Pendleton, K. Vasilev, S. E. Plush and J. D. Hayball, *C*, 2017, **3**, 18.
17 F. Ge, M.-M. Li, H. Ye and B.-X. Zhao, *J. Hazard. Mater.*, 2012, **211**, 366–372.
18 A.-F. Ngomsik, A. Bee, M. Draye, G. Cote and V. Cabuil, *C. R. Chim.*, 2005, **8**, 963–970.
19 B. Boruah, P. K. Samantaray, G. Madras, J. M. Modak and S. Bose, *Chem. Eng. J.*, 2020, 124777.
20 M. Heiranian, A. B. Farimani and N. R. Aluru, *Nat. Commun.*, 2015, **6**(1), 1–6.
21 S. Zinadini, A. A. Zinatizadeh, M. Rahimi, V. Vatanpour and H. Zangeneh, *J. Membr. Sci.*, 2014, **453**, 292–301.
22 X. Yang, J. Li, T. Liang, C. Ma, Y. Zhang, H. Chen, N. Hanagata, H. Su and M. Xu, *Nanoscale*, 2014, **6**, 10126–10133.
23 M. Hu and B. Mi, *Environ. Sci. Technol.*, 2013, **47**, 3715–3723.
24 V. Chandra, J. Park, Y. Chun, J. W. Lee, I.-C. Hwang and K. S. Kim, *ACS Nano*, 2010, **4**, 3979–3986.
25 R. Joshi, P. Carbone, F.-C. Wang, V. G. Kravets, Y. Su, I. V. Grigorieva, H. Wu, A. K. Geim and R. R. Nair, *Science*, 2014, **343**, 752–754.

Open Access Article. Published on 06 May 2020. Downloaded on 2/23/2026 7:28:33 PM.
This article is licensed under a Creative Commons Attribution-NonCommercial 3.0 Unported Licence.

26 J. Lee, H.-R. Chae, Y. J. Won, K. Lee, C.-H. Lee, H. H. Lee, I.-C. Kim and J.-m. Lee, *J. Membr. Sci.*, 2013, **448**, 223–230.
27 W. Li, Y. Yang, J. K. Weber, G. Zhang and R. Zhou, *ACS Nano*, 2016, **10**, 1829–1835.
28 W. Hirunpinyopas, E. Prestat, S. D. Worrall, S. J. Haigh, R. A. Dryfe and M. A. Bissett, *ACS Nano*, 2017, **11**(11), 11082–11090.
29 P. K. Samantaray, S. Baloda, G. Madras and S. Bose, *Adv. Sustainable Syst.*, 2019, 1800153.
30 S. Maiti, P. K. Samantaray and S. Bose, *Nanoscale Adv.*, 2020, **2**(5), 1993–2003.
31 Z. Wang, Q. Tu, S. Zheng, J. J. Urban, S. Li and B. Mi, *Nano Lett.*, 2017, **17**, 7289–7298.
32 J. A. Willcox and H. J. Kim, *ACS Nano*, 2017, **11**, 2187–2193.
33 M.-N. Li, X.-F. Sun, L. Wang, S.-Y. Wang, M. Z. Afzal, C. Song and S.-G. Wang, *Desalination*, 2018, **436**, 107–113.
34 J. H. An and J. Jang, *Nanoscale*, 2017, **9**, 7483–7492.
35 M. Pumera and A. H. Loo, *TrAC, Trends Anal. Chem.*, 2014, **61**, 49–53.
36 V. Agarwal and K. Chatterjee, *Nanoscale*, 2018, **10**, 16365–16397.
37 B. Mondal, A. Mahendranath, A. Som, S. Bose, T. Ahuja, A. A. Kumar, J. Ghosh and T. Pradeep, *Nanoscale*, 2018, **10**, 1807–1814.
38 L. Hu, Y. Ren, H. Yang and Q. Xu, *ACS Appl. Mater. Interfaces*, 2014, **6**, 14644–14652.
39 Y. Tan, P. Liu, L. Chen, W. Cong, Y. Ito, J. Han, X. Guo, Z. Tang, T. Fujita and A. Hirata, *Adv. Mater.*, 2014, **26**, 8023–8028.
40 G. Guan, S. Zhang, S. Liu, Y. Cai, M. Low, C. P. Teng, I. Y. Phang, Y. Cheng, K. L. Duei and B. M. Srinivasan, *J. Am. Chem. Soc.*, 2015, **137**, 6152–6155.
41 V. Agarwal, N. Varghese, S. Dasgupta, A. Sood and K. Chatterjee, *Chem. Eng. J.*, 2019, **374**, 254–262.
42 X. Li and H. Zhu, *J. Materiomics*, 2015, **1**, 33–44.
43 L. Chen, Y. Feng, X. Zhou, Q. Zhang, W. Nie, W. Wang, Y. Zhang and C. He, *ACS Appl. Mater. Interfaces*, 2017, **9**, 17347–17358.
44 G. Eda, H. Yamaguchi, D. Voiry, T. Fujita, M. Chen and M. Chhowalla, *Nano Lett.*, 2011, **11**, 5111–5116.
45 N. I. Taib, V. Agarwal, N. M. Smith, R. C. Woodward, T. G. S. Pierre and K. S. Iyer, *Mater. Chem. Front.*, 2017, **1**, 2335–2340.
46 V. Agarwal, D. McLean, J. Horne, D. Richardson and K. Stack, *J. Appl. Polym. Sci.*, 2013, **127**, 3970–3979.
47 V. Agarwal, A. G. Panicker, S. Indrakumar and K. Chatterjee, *Int. J. Biol. Macromol.*, 2019, **133**, 382–390.
48 B. Bhushan, P. Dubey, S. U. Kumar, A. Sachdev, I. Matai and P. Gopinath, *RSC Adv.*, 2015, **5**, 12078–12086.
49 F. Jiang, J. Xiong, W. Zhou, C. Liu, L. Wang, F. Zhao, H. Liu and J. Xu, *J. Mater. Chem. A*, 2016, **4**, 5265–5273.
50 J. Ryou, Y.-S. Kim, K. Santosh and K. Cho, *Sci. Rep.*, 2016, **6**, 29184.
51 V. M. Boddu, K. Abburi, J. L. Talbott, E. D. Smith and R. Haasch, *Water Res.*, 2008, **42**, 633–642.
52 T. Yoshida, T. Yamaguchi, Y. Iida and S. Nakayama, *J. Nucl. Sci. Technol.*, 2003, **40**, 672–678.
53 F. Edition, *WHO Chron.*, 2011, **38**, 104–108.
54 S. Liu, T. H. Zeng, M. Hofmann, E. Burcombe, J. Wei, R. Jiang, J. Kong and Y. Chen, *ACS Nano*, 2011, **5**, 6971–6980.
55 P. K. Samantaray, G. Madras and S. Bose, *Adv. Sustainable Syst.*, 2019, **3**(10), 1900017.
56 P. K. Samantaray and S. Bose, *Proc. Indian Natl. Sci. Acad.*, 2018, **84**, 669–679.
57 P. K. Samantaray, G. Madras and S. Bose, *ACS Sustainable Chem. Eng.*, 2018, **7**, 1580–1590.
58 V. Agarwal, E. S. Tjandra, K. S. Iyer, B. Humfrey, M. Fear, F. M. Wood, S. Dunlop and C. L. Raston, *Toxicol. Res.*, 2014, **3**, 223–227.
59 P. K. Samantaray, G. Madras and S. Bose, *ChemistrySelect*, 2017, **2**, 7965–7974.
60 N. Padmavathy, P. K. Samantaray, L. D. Ghosh, G. Madras and S. Bose, *Nanoscale*, 2017, **9**, 12664–12676.
61 V. Agarwal, P. Toshniwal, N. E. Smith, N. M. Smith, B. Li, T. D. Clemons, L. T. Byrne, F. Kakulas, F. M. Wood and M. Fear, *Chem. Commun.*, 2016, **52**, 327–330.
62 V. Agarwal, F. M. Wood, M. Fear and K. S. Iyer, *Aust. J. Chem.*, 2017, **70**, 280–285.

 This journal is © The Royal Society of Chemistry 2020